Supporting Information to: Variable-Temperature Tip-Enhanced Raman Spectroscopy of Single-Molecule Fluctuations and Dynamics

Kyoung-Duck Park,† Eric A. Muller,† Vasily Kravtsov,† Paul M. Sass,† Jens Dreyer,‡ Joanna M. Atkin,† and Markus B. Raschke*,†

†*Department of Physics, Department of Chemistry, and JILA, University of Colorado, Boulder, CO, 80309, USA*

‡*German Research School for Simulation Sciences, RWTH Aachen University and Forschungszentrum Jülich, D-52425 Jülich, Germany*

¶*Department of Chemistry, University of North Carolina, Chapel Hill, NC 27599*

Received December 22, 2015; E-mail: markus.raschke@colorado.edu

Sample Preparation and Characterization

Tip-enhanced Raman spectroscopy (TERS) and micro-Raman are both used to observe spectra of malachite green (MG) in sub-monolayer thin fiilms. We calibrate adsorbate thickness by preparing ultra-thin films of different submonolayer coverage. MG solutions of varying concentration in ethanol are spin-coated at a fixed rate of 3000 rotations per minute onto glass microscope slides. Visible absorption spectra of the MG coated glass, shown in Figure 1a are measured by a UV-vis-NIR spectrophotometer in transmission mode (Cary 500 Varian), and coverage is calibrated by the known optical cross section of MG. Visible absorption spectra show a linear relationship between solution concentration and film thickness of spin-coated samples at the constant spin-coating speed over the investigated range MG concentrations. Thicknesses were measured for ultrathin films between 1 monolayer and the lowest coverages measurable by UV-vis spectroscopy corresponding to ∼0.05 monolayers. MG solution concentration for TERS was controlled to produce a coverage of ∼0.006 monolayers, corresponding to an average of 1-2 molecules under the tip, while coverages for micro-Raman were increased to allow sufficient signal-to-noise in far-field data collection.

We characterize the tip-sample geometry by independently imaging the tip and sample. Scanning electron microscope images (Figure S1c) show the expected 20 nm tip radius and a relatively smooth tip geometry for the etched Au tips. We collect high-resolution atomic force microscopy images of the sample using silicon tips (Super-Sharp Silicon, NanoWorld, 285 kHz resonance) with nominal tip radius of 2 nm, operated in intermittent contact mode. AFM images (Figure S1d) show the roughness of the polycrystalline template-stripped Au. Typical RMS roughness is $\leq$0.5 nm, and the roughness shown in Figure S1d is 0.35 nm, although individual grains are found to have a small lateral extent. The large area roughness of template stripped Au is also found to be small, with the range of roughness being $\leq$5 nm in a 10 μm image.

MG ultra-thin films consist of randomly distributed molecular adsorbate. In order to locate the regions which contain a small-ensemble of MG rather than larger clusters, several TERS spectra were recorded at each temperature, and the narrowest spectra at each temperature were used. Figure 1b contains repeated TERS spectra at 90 K, showing the expected narrower linewidths (blue) in sub-ensemble or single-molecule spectra relative to a broader linewidth, which may result from spectra collected from a larger MG cluster. Fluctuations attributed to rotation and conformational changes discussed in the main text were only observed in the narrowest spectra at 90 K.

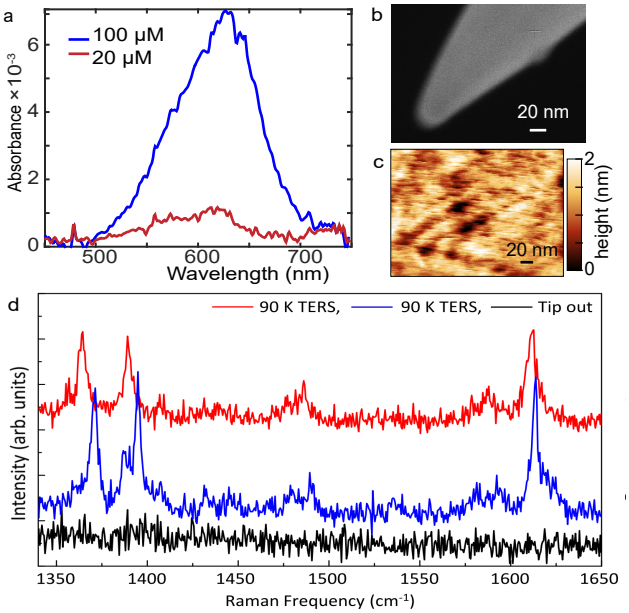

Figure 1. (a) UV-vis spectra of MG spin-coated on glass are used to calibrate thin-film thickness. (b) Scanning electron microscope image showing AFM tip geometry (c) AFM image of Au substrate imaged with a sharp tip in intermittent contact mode. (b) Comparison of low temperature TERS spectra at different locations across the sample.

Comparison between TERS and micro-Raman

Here we present a through comparison between the temperature dependent TERS and micro-Raman spectroscopy. In order to facilitate a detailed comparison between spectral line shapes in the ensemble-averaged micro-Raman and TERS spectra, spectra for both methods are collected with the same apparatus, with the Au tip brought close to the surface or retracted, respectively. By using same excitation laser, collection optics, and detector, we minimize systematic differences between each method and maintain the spectral resolution of 1.2 cm^{-1}.

Figure 2a shows a comparison between micro-Raman and TERS spectra under identical experimental conditions. Because the range of the charge-coupled device detector is less than the full frequency region of interest, spectra of the full region are collected by superimposing two overlapping spectral regions. The peaks in the micro-Raman spectra narrow when the temperature decreased from 300 K to 90 K,

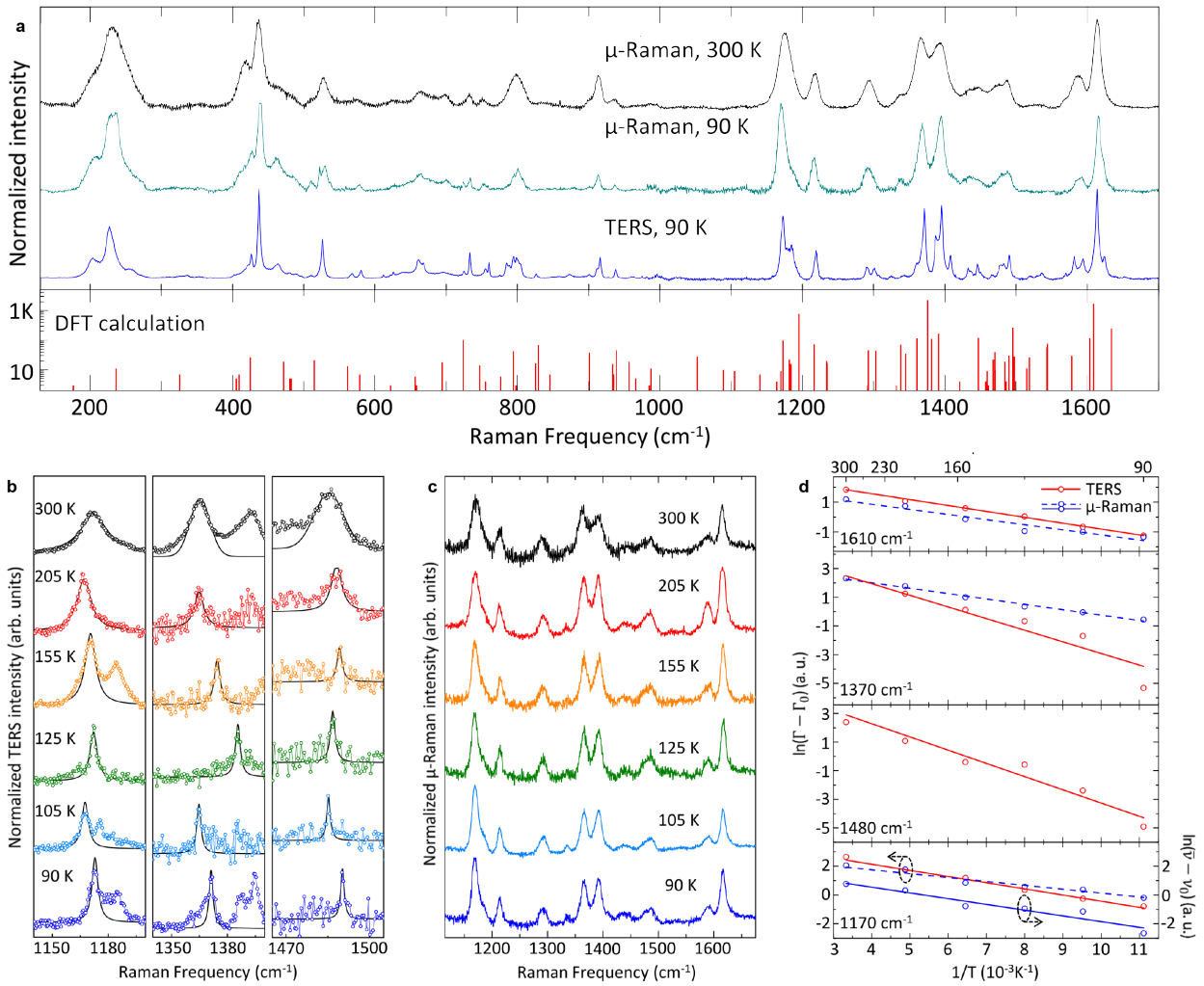

Figure 2. (a) Comparison between spectra: micro-Raman spectra at 300 K, micro-Raman spectra at 90 K, and TERS spectra at 90 K. Bottom, density functional theory calculation exhibiting predicted Raman modes over the full spectral range. (b) Lorentzian line fit analysis of the temperature dependent TERS spectra of MG exhibiting peak narrowing for the peaks at 1170, 1370, and 1480 cm^{-1}. Lorentzian fits for the peak at 1610 cm^{-1} are shown in Figure 1c of the main text. (c) Temperature dependent micro-Raman spectra. Spectra are background subtracted and intensity normalized. (d) Arrhenius plot of $\ln(\Gamma(T) - \Gamma_0)$ and $\ln(\bar{\nu}(T) - \bar{\nu}_0)$ versus $1/T$. Data are identical to the ones shown in Figure 2 of the main text.

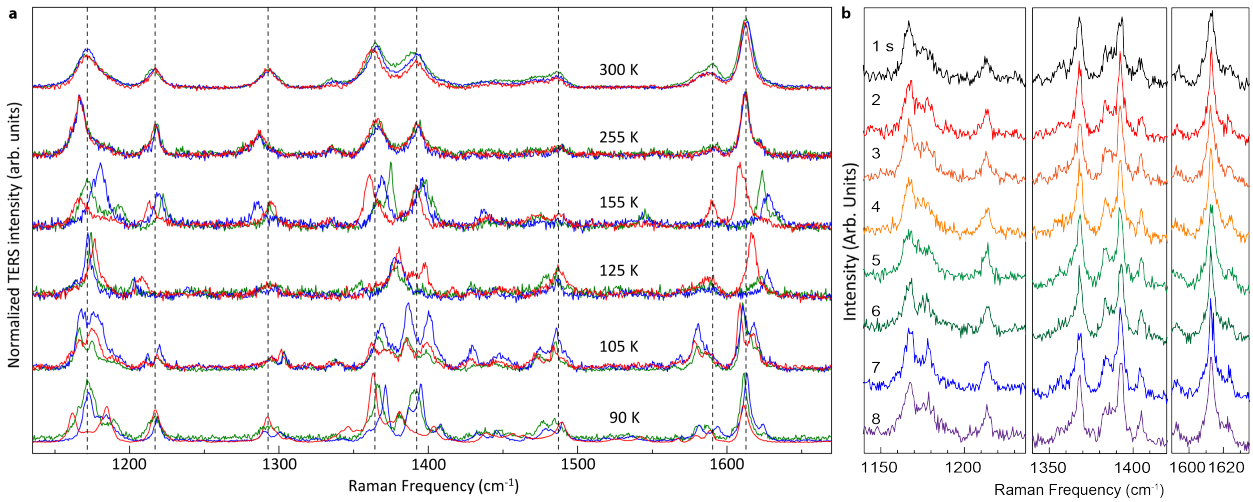

Figure 3. (a) Repeated TERS spectra of MG taken at each temperature in the region 90-300 K. Sample inhomogeneity and spectral fluctuations result in significant variation in peak position between the macroscopic areas of the sample. Spectra from different TERS acquisitions under identical sample conditions are identified by color (red, green, blue) and offset to distinguish spectra collected at different temperatures. (b) Time-series TERS spectra at 90 K in the high frequency region with 1 s integration times. TERS spectra of this frequency range were not observed to fluctuate under the conditions used.

however the TERS peaks narrow by a significantly greater amount (Figure 2b). Quantitative comparison with density functional theory (DFT) calculations (bottom of Figure 2a) allows assignment of vibrational modes in the 90 K TERS spectrum, which is more challenging for the micro-Raman or 300 K TERS spectra. The intensities of several Raman active modes are not accurately described by DFT. This is expected from the rotationally averaged DFT polarizability calculations, which do not account for adsorbate geometry, interactions with the substrate, electronic contributions to polarizability or intermolecular interactions in the dense sample used in micro-Raman measurements.

Temperature dependent peak positions and peak widths are measured for four peaks. Figure 2b shows Lorentzian fits for each of the 1170, 1370 and 1480 cm^{-1} peaks (fits for the 1610 cm^{-1} peak are shown in the main text). The narrowest spectra with 1-10 s acquisition are selected from the full data set. By selecting the spectra with minimal inhomogeneous broadening within the short acquisition time, TERS spectra are obtained from regions containing only a few or single molecules.

Table 1. Results from Arrhenius fits to the temperature dependent micro-Raman linewidth $\Gamma(T)$ for three selected peaks over the temperature range 90-300 K.

Peak (cm^{-1})	E_A (cm^{-1})	Γ_0 (cm^{-1})	A (cm^{-1})
ν(1610)	270 ± 60	9.9 ± 0.3	12 ± 3
ν(1370)	280 ± 30	10.8 ± 0.3	39 ± 5
ν(1170)	120 ± 40	8.5 ± 0.9	20 ± 1

In contrast to the pronounced narrowing in low temperature TERS, the micro-Raman spectra narrow only slightly as a function of temperature. Figure 2c shows micro-Raman spectra for each temperature. Three peaks of temperature dependent micro-Raman spectra are fit to Lorentzian line shapes in the same manner as the temperature dependent TERS spectra. The peak at 1480 cm^{-1} could not be fit accurately at all temperatures in the micro-Raman spectra. Temperature dependent fits to peak position and linewidth are shown on a logarithmic Arrhenius plot in Figure 2d and a linear plot in Figure 2 of the main text. The exponential temperature dependence of $\ln(\Gamma - \Gamma_0)$ is seen more clearly in the linear fits of Figure 2d.

Fitting results for temperature-dependent miro-Raman are summarized in Table S1. Comparison of the micro-Raman to TERS fits reveals different temperature dependences. The activation energy E_A and prefactor A in micro-Raman are much smaller than in TERS, while Γ_0 is 3-5 times wider in micro-Raman. Inhomogeneously broadened peaks can contain multiple unresolved modes at nearby frequencies, and narrowing of individual modes can be masked by the presence of the multiple modes or by heterogeneity greater than the homogeneous linewidth. Micro-Raman spectroscopy thus underestimates E_A and $\delta\bar{\nu}(T)$ as expected.

Low Temperature Rotational Motion and Spectral Fluctuations

At room temperature, fast molecular motions blur the spectral signatures for even a single molecule. At cryogenic temperatures, rotational motion and spectral fluctuations are slowed to the timescale of seconds.

Figure 3a shows TERS spectra repeatedly collected at each temperature between 300 K and 90 K with acquisition times ≥20 s. Between the measurements, the tip is retracted several μm and brought back in to a different location on the sample. At 300 K and 255 K thermally broadened peaks are well reproduced by repeated TERS measurements, while at 155-90 K individual peaks appear to shift in a random manner between the acquisitions. Spectral fluctuations at room temperature occur faster than the timescale of the spectral acquisition, resulting in the appearance of inhomogeneously broadened peaks even from a small sample volume. In contrast, slowed or frozen spectral fluctuations appear as an inhomogeneity across the sample and between spectral acquisitions, which we observe as heterogeneity between spectral acquisitions only at low temperatures. Under the conditions investigated, however, TERS spectra of the high frequency region with short acquisition times of 1 s, shown in Figure 3b were not observed to fluctuate significantly in either intensity or frequency.

In contrast to the high frequency region, low temperature TERS spectra of the low frequency region show significant fluctuations of certain peaks, as discussed in relation to Figure 3-4 of the main text. We present additional data of the low frequency region, with the full time-series collected over 209 s shown in Figure 4a. Fluctuations in total intensity and fluorescence background are observed in addition to fluctuations in intensity of individual modes. Zoomed-in spectra are shown (right of Figure 4a) from the areas indicated by red, yellow, and green dashed boxes. Time-series spectra over the full time range show both the anti-correlated intensity fluctuations associated with rotational motion as well as the slower spectral fluctuations. Covariance plots shown in Figure 3b and Figure 4b of the main text are taken from the regions indicated by white dotted areas in Figure 4a.

The peak positions of near ∼ 435, ∼ 525, and ∼ 800 cm^{-1} shift by several cm^{-1} between each of the short time segments. Figure 4b shows TERS spectra integrated over each of these time segments. Since the frequencies of a number of modes shift coincidently, quantitative peak assignment is still possible by comparing the full TERS spectrum with calculated DFT Raman frequencies (bottom).

Only certain modes are observed to shift between different frequencies. Figure 5a shows the time evolution of peak position over in the time range of 37-72 s from fits to several peaks. Several peaks, shown in red and blue, alternate in intensity (525 versus 528 cm^{-1} and 799 versus 804 cm^{-1}). Over the same time period, the mode at 580 cm^{-1} with A_1 symmetry assignment (black) shifts only slightly in frequency and does not undergo blinking during the frequency jumps. Figure 5b-c show two peaks which show similar behavior over this same time period. The overall intensity of these peaks changes randomly over this time period, and these peaks do not disappear or change intensity or frequency in a systematic manner during the frequency jumps of the fluctuating modes. As discussed in the main text, a number of modes are stable in both intensity and frequency over the same time-series acquisition during which other modes undergo sharp jumps in both frequency and intensity. These stable modes serve as an ideal reference to clearly demonstrate that of only particular normal modes can only result from the intrinsic molecular response rather than detection artifacts or extrinsic effects.

Figure 6a shows the correlation plot corresponding to the covariance plot shown in Figure 3b of the main text. The frequency correlation, $\chi_{ij} = \sigma_{ij}/(\sigma_{ii}\sigma_{jj})$, shows normalized intensities as compared to the covariance plots shown in the main text. The normalized frequency correlation map enables quantification of correlation or anti-correlation, al-

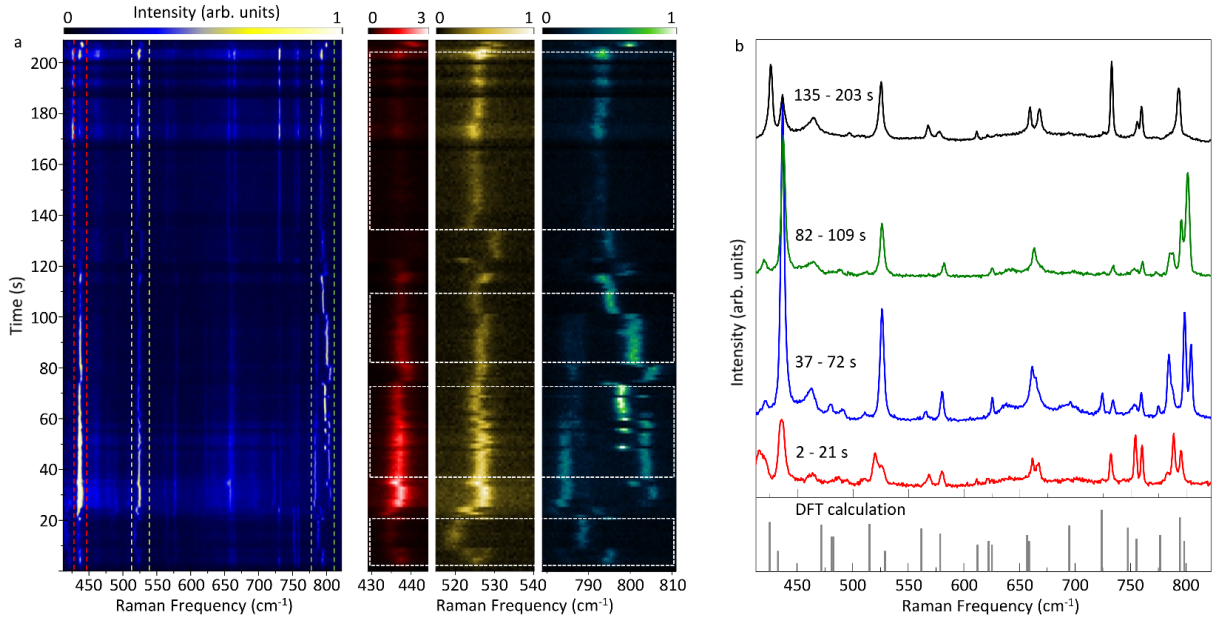

Figure 4. (a) Time-series TERS spectra taken at 1 s intervals, showing the full acquisition time of 209 s and full range of the spectrometer. Right, zoomed-in regions showing both rotational motion and spectral fluctuations over the full time-series. (b) TERS spectra averaged over short time integrals from the time-series data in (a). TERS peak positions are compared with DFT calculated normal mode frequencies and intensities, shown on a logarithmic scale (Bottom).

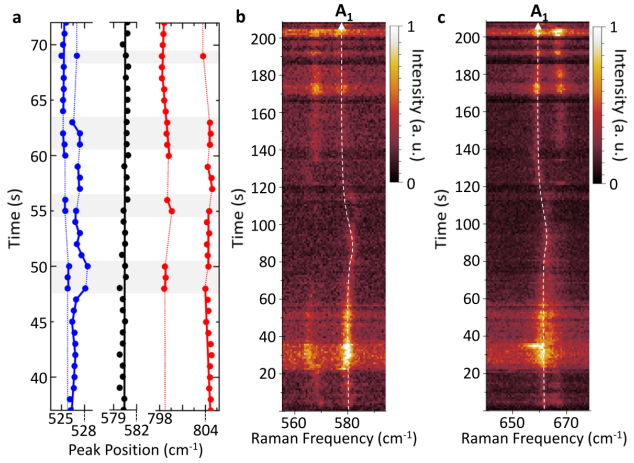

Figure 5. (a) Center frequency of three different vibrational modes during 37-72 s. Time-series TERS spectra for the 580 cm^{-1} (b) and 660 cm^{-1} (c) taken at 1 s intervals, showing the full acquisition time of 209 s.

though the line shape of each peak is obscured by this normalization. As noted in the main text, the correlation plot shows that peaks assigned to orthogonal A_2 and B_1 symmetries have correlations of +1 with modes of the same symmetry character and -1 with modes with different symmetry over this time period. Other spectral ranges and time-periods similarly show correlation and anti-correlation of A_2 and B_1 modes with magnitudes of $|\pm 0.6$ to $1|$. As expected, peaks of fully symmetric A_1 character fluctuate less in intensity and are found to be correlated with all other peaks and with intensity fluctuations of the non-resonant background signal.

Figure 6b-d show covariance plots for each short time segment, showing a larger region of interest than Figure 4b of the main text. In the covariance plots spanning a larger frequency region, both correlation and anti-correlation are clearly observed for peaks separated by several hundred cm^{-1}. Anti-correlated TERS intensities are seen between A_2 modes and B_1 modes at $\sim$ 435, $\sim$ 525, and $\sim$ 800 cm^{-1} in Figure 6b-c. Peaks are labeled by their frequency over the time range as shown in Figure 3b of the main text. Spectral fluctuations cause the slight shift of peak positions between each short-time covariance plot. No fluctuations are observed in the final time segment shown in Figure 6d, corresponding to a static molecular position. Although the explicit causes of spectral fluctuations cannot be concluded here, a number of possible changes in substrate-adsorbate interaction could contribute to frequency fluctuations, including alternately bonding to defects such as atomic vacancies, step edges, or terrace sites.

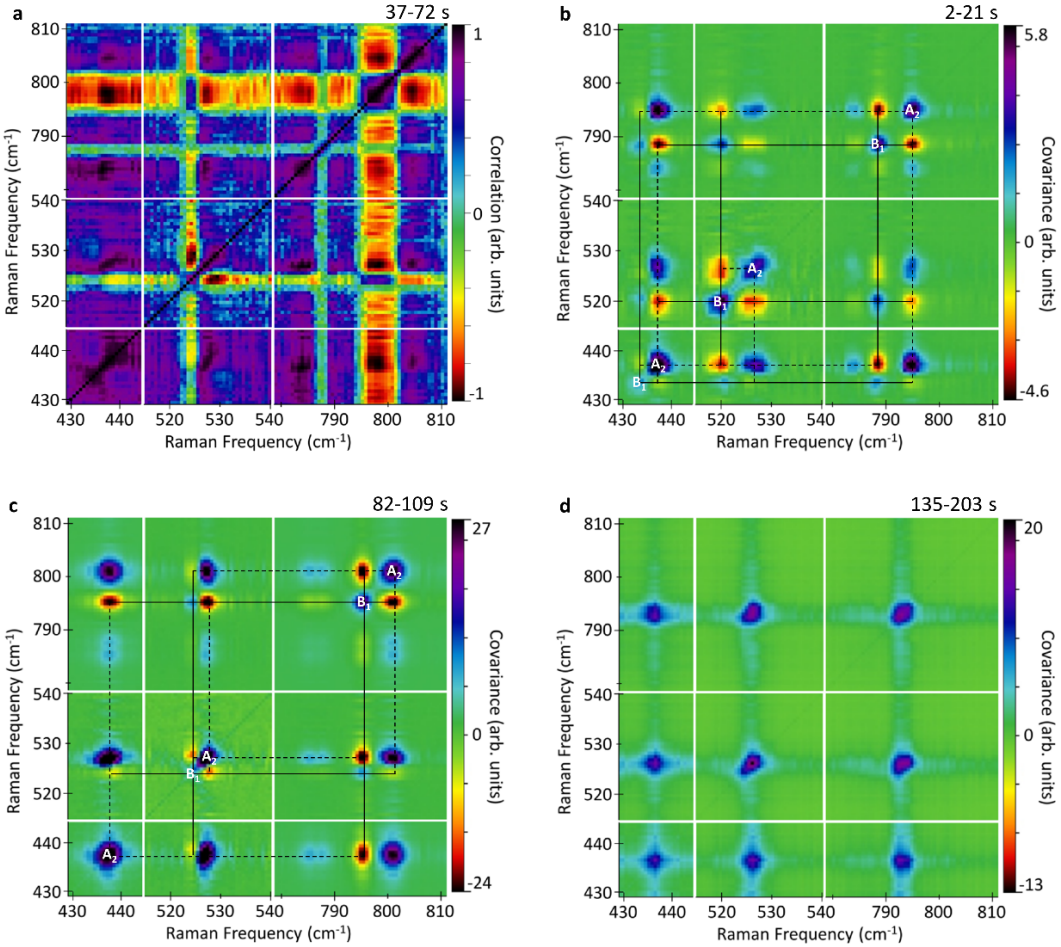

Figure 6. (a) Correlation plot of Raman intensity for the time region 37-72 s (covariance plot is shown in Figure 3b of the main text). Covariance plots of Raman intensity over three time regions (b) 2-23 s, (c) 82-109 s, and (d) 135-203 s.